Structure
Article

# The Free Energy Landscapes Governing Conformational Changes in a Glutamate Receptor Ligand-Binding Domain

Albert Y. Lau[1] and Benoît Roux[1,*]
[1]Institute for Molecular Pediatric Sciences, Department of Biochemistry and Molecular Biology, Ellen and Melvin Gordon Center for Integrative Science, The University of Chicago, 929 East 57th Street, Chicago, IL 60637, USA
*Correspondence: roux@uchicago.edu
DOI 10.1016/j.str.2007.07.015

## SUMMARY

**Ionotropic glutamate receptors are ligand-gated transmembrane ion channels activated by the binding of glutamate. The free energy landscapes governing the opening/closing of the GluR2 S1S2 ligand-binding domain in the apo, DNQX-, and glutamate-bound forms are computed by using all-atom molecular dynamics simulations with explicit solvent, in conjunction with an umbrella sampling strategy. The apo S1S2 easily accesses low-energy conformations that are more open than observed in X-ray crystal structures. A free energy of 9–12 kcal/mol becomes available upon glutamate binding for driving conformational changes in S1S2 associated with receptor activation. Small-angle X-ray scattering profiles calculated from computed ensemble averages agree better with experimental results than profiles calculated from static X-ray crystal structures. Water molecules in the cleft may contribute to stabilizing the apo S1S2 in open conformations. Free energy landscapes were also computed for the glutamate-bound T686A and T686S S1S2 mutants, and the results elaborate on findings from experimental functional studies.**

## INTRODUCTION

Ligand-gated ion channels mediate information transfer across cell membranes. Ionotropic glutamate receptors (iGluRs) are ligand-gated ion channels that reside in the membrane of the postsynaptic neuron. iGluRs are abundantly expressed in the brain and spinal cord, and they mediate excitatory responses at the vast majority of central nervous system (CNS) synapses in higher vertebrates (Dingledine et al., 1999). iGluRs are important in the development and function of the CNS and in the formation of synaptic plasticity, which underlies memory and learning (Asztely and Gustafsson, 1996; Cull-Candy et al., 2006; Isaac et al., 2007). Dysfunction in iGluRs is implicated in a range of diseases and injuries, including stroke, epilepsy, schizophrenia, depression, Rasmussen's encephalitis, amyotrophic lateral sclerosis, Alzheimer's disease, Huntington's disease, and Parkinson's disease (Bräuner-Osborne et al., 2000; Dingledine et al., 1999; Hollmann and Heinemann, 1994; Kristiansen et al., 2007; O'Neill et al., 2004; O'Neill and Witkin, 2007; Rogers et al., 1994).

The extracellular ligand-binding domain of these receptors responds to the binding of the neurotransmitter glutamate (agonist) by undergoing a conformational change that opens cation-permeable channels (activation), thereby transducing chemical signals from the presynaptic neuron into electrical impulses in the postsynaptic cell. After activation, the agonist either dissociates from the ligand-binding domain, and the receptor returns to the resting state (deactivation), or the agonist remains bound, but the channel closes as a result of conformational changes in the receptor that decouple agonist binding from activation (desensitization) (Armstrong et al., 2006). X-ray crystallography has revealed that the portion of iGluRs that binds agonists is composed of two discontinuous polypeptide segments called S1 and S2 (Stern-Bach et al., 1994) that, when linked together, fold into a bilobate, or "clamshell"-like, structure known as the S1S2 ligand-binding core (Armstrong et al., 1998; Kuusinen et al., 1995). iGluR subunits assemble into tetramers in vivo, and S1S2 has been suggested to assemble as a dimer-of-dimers (Armstrong and Gouaux, 2000; Ayalon and Stern-Bach, 2001; Nakagawa et al., 2005; Schorge and Colquhoun, 2003; Tichelaar et al., 2004).

iGluRs have been the subject of intense study, and a wealth of insight has been gained into the structure (Armstrong et al., 2006; Holm et al., 2005; Madden, 2002; Madden et al., 2005; Mayer, 2006; McFeeters and Oswald, 2004; Nakagawa et al., 2005; Ramanoudjame et al., 2006; Speranskiy and Kurnikova, 2005; Tichelaar et al., 2004) and dynamics (Ahmed et al., 2007; Arinaminpathy et al., 2006; Cheng et al., 2005; Mamonova et al., 2005; Mendieta et al., 2005; Valentine and Palmer, 2005) of the S1S2 ligand-binding core. For instance, X-ray crystal structures of the apo and ligand-bound complexes have revealed the fundamental conformational change underlying iGluR function. The binding core, open in the absence of a bound ligand, closes in a clamshell-like fashion upon ligand binding. The energetic factors governing such conformational

  

changes, however, have yet to be revealed. Though very informative, X-ray crystal structures of the apo and ligand-bound complexes can only provide a static view of the most stable conformational state of the system. Knowledge of the free energy landscape governing the thermodynamic equilibrium among various accessible conformations is required in order to understand how the receptor functions. For instance, a straightforward question such as—how much useful free energy becomes available for driving the conformational changes associated with receptor activation upon ligand binding?—has not been answered. One reason is that the microscopic factors controlling the conformational energetics of the ligand-binding domain cannot be readily extracted from experiments, as they require consideration of conformational states that are inherently transient or not strongly populated. Molecular dynamics (MD) simulations based on detailed atomic models present a rich avenue by which to start addressing these issues.

Simple ''brute force'' simulations are, however, somewhat limited in the case of complex macromolecular systems such as iGluRs, which undergo significant conformational changes. These difficulties are further compounded by the fact that a quantitative analysis of energetic factors underlying iGluR function necessitates a comparison of the relative free energy of several conformational states (open/closed with/without bound ligand), some of which are expected to be of marginal stability (e.g., open with bound ligand and closed without bound ligand). A more promising strategy for obtaining quantitatively meaningful results that can be compared with experimental data is to consider the ''free energy landscape,'' or ''potential of mean force'' (PMF), along specifically chosen coordinates called ''order parameters'' that report the conformation of a macromolecular system (for example, see Banavali and Roux, 2005; Huang et al., 2003; Ravindranathan et al., 2005). The relative free energy between two or more states is a measure of the probability of finding the system in those states. PMF calculations with enhanced sampling methods along multidimensional order parameters are effective means of studying relatively rare, i.e., on the microsecond-millisecond timescale (Ahmed et al., 2007; Cheng et al., 2005; Valentine and Palmer, 2005), and complex molecular motions governing biological function. Umbrella sampling computations correspond to simulations in which one or several biasing potentials have been introduced to help accelerate the convergence of configurational sampling (Torrie and Valleau, 1977). The distribution functions from all sampling windows are then unbiased and recombined to obtain the final estimate of the PMF by using the weighted histogram analysis method (WHAM) (Kumar et al., 1992; Souaille and Roux, 2001).

In the present study, we used all-atom MD simulations with explicit solvent, in conjunction with an umbrella sampling strategy, to compute the free energy landscapes, described by the PMFs, governing the opening or closing of the α-amino-3-hydroxy-5-methyl-4-isoxazole propionic acid (AMPA)-sensitive GluR2 S1S2 core in the apo, 6,7-dinitro-2,3-quinoxalinedione (DNQX)-bound, and glutamate-bound forms. AMPA is a full agonist of GluR2, and DNQX is an antagonist. The apo S1S2 is found to easily adopt conformations that are more open than has been observed in X-ray crystal structures (within ~0.5 kcal/mol from the free energy minimum). A free energy of 9–12 kcal/mol becomes available upon glutamate binding for driving the conformational changes in S1S2 associated with receptor activation: the free energy is 9 kcal/mol if the ligand initially docks in the ligand-binding cleft while the latter is in the apo S1S2 crystal structure conformation, or 12 kcal/mol if the ligand docks in a more open cleft. Features in the glutamate-bound S1S2 free energy landscape suggest a sequence of interactions in the cleft that correspond to different states of cleft closure. Ensemble average small-angle X-ray scattering (SAXS) profiles calculated from the free energy landscapes agree closely with experimental profiles (Madden et al., 2005). A cluster of water molecules in the cleft may contribute to stabilizing the apo S1S2 in an open conformation. The free energy landscapes governing the opening or closing of glutamate-bound T686A and T686S S1S2 mutants were also computed and were found to agree qualitatively with experimental functional studies (Robert et al., 2005).

## RESULTS AND DISCUSSION

### Free Energy Landscapes

Free energy landscapes computed by using umbrella sampling methods depend on the (somewhat arbitrary) choice of order parameter used to describe the conformational change of interest. Nonetheless, this choice becomes critical only when one aims to compute the kinetic rate between stable states (or basins). In this study, we do not characterize kinetic rates of conformational changes. Our primary goal in computing these free energy landscapes is to determine the relative differences in free energy among conformational states (the quantity that governs conformational changes) and the equilibrium populations of these states. The equilibrium populations among well-defined stable states are independent of the choice of order parameter as long as the order parameter accurately distinguishes these states.

To monitor the thermodynamics of the opening and closing of the S1S2 core, we have identified a two-dimensional (2D) order parameter ($\xi_1$,$\xi_2$) (Figure 1). $\xi_1$ describes the distance between the center-of-mass (COM) of residues 479–481 in Lobe 1 and residues 654–655 in Lobe 2. $\xi_2$ describes the distance between the COM of residues 401–403 in Lobe 1 and residues 686–687 in Lobe 2. In comparing the X-ray crystal structures of apo and agonist-bound S1S2, the distance between T480 and S654 (captured in $\xi_1$) and the distance between E402 and T686 (captured in $\xi_2$) both differ by ~3.5 Å. These two pairs of residues are hydrogen-bonded in the agonist-bound structures. Since $\xi_1$ and $\xi_2$ describe distances across two different edges of the ligand-binding cleft, they describe the relative conformations between Lobes 1 and 2 more effectively than, for example, an angle between the two lobes, which would not necessarily capture a tilt of one

 

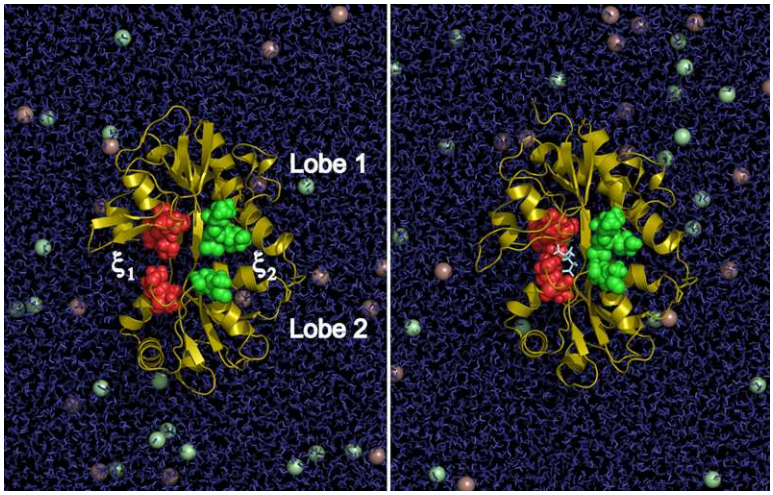


**Figure 1. Representation of GluR2 S1S2 Solvated by a 150 mM NaCl Aqueous Solution**

A 2D order parameter describing the opening or closing of the binding cleft is indicated by the coordinates $\xi_1$ and $\xi_2$. $\xi_1$ describes the distance between the center-of-mass (COM) of residues 479–481 in Lobe 1 and residues 654–655 in Lobe 2 (red spheres). $\xi_2$ describes the distance between the COM of residues 401–403 in Lobe 1 and residues 686–687 in Lobe 2 (green spheres). The crystal structure of the apo S1S2 (PDB ID: 1FTO, chain A) is shown in the left panel, and the crystal structure of the glutamate-bound S1S2 (PDB ID: 1FTJ, chain A) is shown in the right panel. The glutamate ligand in the right panel is shown in stick representation. $Na^+$ and $Cl^-$ ions are shown as purple and green spheres, respectively. For clarity, solvent molecules in front of the protein are not shown.

lobe with respect to the other. S654 and T655 are in the vicinity of a flexible region of Lobe 2 (the peptide bond between D651 and S652 adopts multiple conformations in the crystal structures [Armstrong and Gouaux, 2000]), so local motions might affect the observed $\xi_1$. The effect of local motions, however, is expected to be minimal since the COM of two residues, both of which lie near the beginning of a helix, will be relatively resistant to neighboring fluctuations and should accurately report overall lobe motions. This choice of order parameter is appropriate for distinguishing different degrees of separation between the two lobes and is therefore sufficient for the present study focused on thermodynamic equilibrium factors. The equilibrium free energy landscape that governs conformational transitions in S1S2 for each protein system is presented as a function of this 2D order parameter, $W(\xi_1,\xi_2)$, and also as a function of a one-dimensional (1D) reduced coordinate, $W(\xi_{12})$, where $\xi_{12} = (\xi_1 + \xi_2)/2$. $W(\xi_1,\xi_2)$ and $W(\xi_{12})$ for the apo, DNQX-, and glutamate-bound S1S2 are shown in Figure 2.

The free energy landscape governing the conformation of the apo S1S2 features a broad basin that extends to include conformations of the ligand-binding cleft that are more open than observed in available X-ray crystal structures (Figure 2). According to the calculated free energy landscape, these more open conformations are easily accessible with little energetic cost. The crystal structure of the apo S1S2 is positioned at (12.8 Å, 11.4 Å) for chain A and (12.3 Å, 10.7 Å) for chain B, while the computed global free energy minimum is at (12.1 Å, 11.5 Å). The free energy required to go to conformations of the cleft that are more open than seen in crystal structures, however, is only ~0.5 kcal/mol. It is encouraging to note that, even though the starting conformations for the MD umbrella sampling simulations were generated from the glutamate-bound S1S2 crystal structure (chain A), the deepest free energy minimum appears at the position of the apo crystal structure, and not at the glutamate-bound structure. Since $\mathrm{Prob}(\xi_{12}) \propto \exp[-W(\xi_{12})/k_BT]$, where $\mathrm{Prob}(\xi_{12})$ is the probability of observing a conformation $\xi_{12}$, $k_B$ is Boltzmann's constant, and $T$ is temperature, from $W(\xi_{12})$ (Figure 2B, apo), we estimate that 91% of the conformational ensemble populates the space in which $W(\xi_{12}) \leq 1.0$ kcal/mol, 11.05 Å $\leq \xi_{12} \leq$ 15.35 Å. This conformational range corresponds to a cleft opening of ~16°–30° relative to the glutamate-bound S1S2 crystal structure, determined by using the program HINGEFIND (Wriggers and Schulten, 1997). The crystal structure of the glutamate-bound S1S2 is positioned at (9.5 Å, 7.8 Å) for chain A, (9.5 Å, 7.7 Å) for chain B, and (9.4 Å, 7.8 Å) for chain C. An energy of 4.0 kcal/mol is required for the apo S1S2 to reach this region of conformational space from the X-ray crystal conformation of the apo S1S2. Water molecules occupy the open apo cleft and interact favorably with several residues in the cleft, especially the guanidinium group of R485. These water molecules may stabilize the cleft in open conformations. The binding of ligands to R485 would decrease the cleft's affinity for water, making it easier for the cleft to close.

The DNQX-bound S1S2 free energy landscape is moderately funneled at its global free energy minimum, (12.7 Å, 11.3 Å) (Figure 2). The crystal structure of the DNQX-bound S1S2 is positioned at (12.0 Å, 10.8 Å) for chain A and at (12.3 Å, 10.5 Å) for chain B. The starting conformations for umbrella sampling were generated from the crystal structure of the DNQX-bound S1S2 (chain A). DNQX mediates interactions between Lobes 1 and 2 by interacting with Y450 and R485 in Lobe 1 and T686, E705, and M708 in Lobe 2. These interactions contribute to restricting the range of highly populated conformations to a small region around the free energy minimum. Approximately 86% of the conformational ensemble populates the space in which $W(\xi_{12}) \leq 1.0$ kcal/mol, 11.20 Å $\leq \xi_{12} \leq$ 12.70 Å. 9.2 kcal/mol would be required for the DNQX-bound S1S2 to go from its crystal structure conformation to the closed conformation corresponding to the crystal structure of the glutamate-bound S1S2. This barrier to closing is due to steric clash between DNQX and residues in Lobe 2, particularly E705. DNQX therefore inhibits S1S2 closure, and

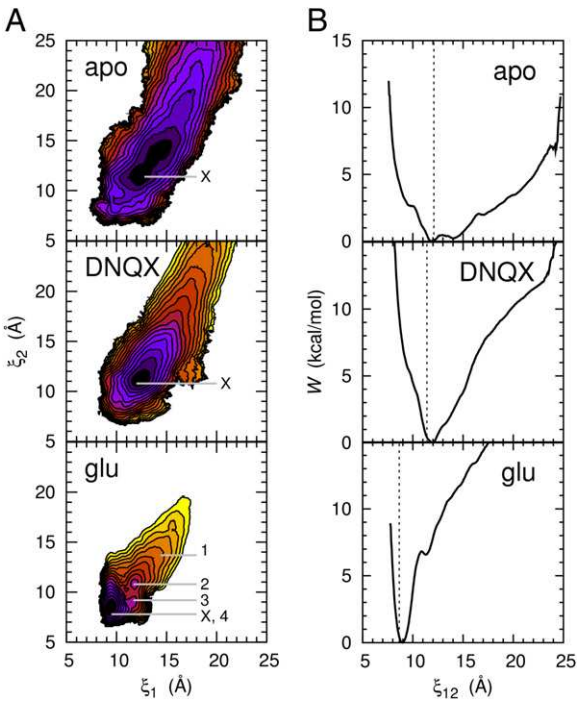


**Figure 2. The Free Energy Landscapes for Conformational Changes in GluR2 S1S2 as Described by the Order Parameter ($\xi_1$,$\xi_2$)**

(A and B) (A) 2D and (B) 1D PMF plots are shown for the apo, DNQX-, and glutamate-bound S1S2. In (A), each color contour corresponds to 1 kcal/mol. The positions marked "x" indicate X-ray crystal structure conformations (only chain A from each crystal structure is marked; the other chains are positioned very close to chain A [see text]). The crystal structure conformation of the AMPA-bound S1S2 is at nearly the identical position as the glutamate-bound S1S2. The positions labeled **1**–**4** in the glu panel correspond to snapshots, shown in Figure 4, of the ligand-binding cleft taken from MD trajectories. In (B), the PMF along the reduced coordinate $\xi_{12} = (\xi_1 + \xi_2)/2$ is shown. The dashed lines indicate the X-ray crystal structure conformations.

transmembrane channel opening, via a "foot-in-the-door" mechanism, as suggested from structural studies (Armstrong and Gouaux, 2000; Mayer, 2006).

The glutamate-bound S1S2 free energy landscape features a narrow and deep basin at (9.4 Å, 8.4 Å), where the computed global free energy minimum is located (Figure 2). The crystal structure of the glutamate-bound S1S2 is positioned at (9.5 Å, 7.8 Å) for chain A, (9.5 Å, 7.7 Å) for chain B, and (9.4 Å, 7.8 Å) for chain C. The crystal structure of the AMPA-bound S1S2 is similarly positioned at (9.3 Å, 7.8 Å) for chain A, (9.3 Å, 7.8 Å) for chain B, and (9.3 Å, 7.9 Å) for chain C. The starting conformations for umbrella sampling were generated from the glutamate-bound S1S2 crystal structure (chain A). Approximately 94% of the conformational ensemble populates the space in which $W(\xi_{12}) \leq 1.0$ kcal/mol, 8.50 Å $\leq \xi_{12} \leq$ 9.45 Å. The numerous hydrogen bonds formed between the glutamate ligand and each of the two lobes, as well as hydrogen bonds formed directly between the two lobes, contribute to the restricted range of highly populated conformations. State **1**, at (14.4 Å, 13.7 Å), corresponds to a low-energy conformation for the apo S1S2 that is more open than observed in crystal structures. A metastable substate is observed at (11.7 Å, 10.8 Å) (Figure 2A, glu, state **2**), which is near the location of the global free energy minima in both the apo and DNQX-bound S1S2 free energy landscapes. The lowest free energy pathway from state **2** to the fully closed state at (9.4 Å, 8.4 Å), state **4**, traverses an intermediate state, state **3**. The position of **3** with respect to **2** and **4** suggests that complete cleft closure occurs by Lobes 1 and 2 coming together first primarily along $\xi_2$, in going from **2** to **3**, followed by $\xi_1$, in going from **3** to **4**. Conversely, when the glutamate-bound S1S2 is in **4**, cleft opening occurs reversibly by the lobes separating first primarily along $\xi_1$, followed by $\xi_2$. A remarkable amount of free energy becomes available for driving cleft closure upon binding a glutamate ligand: the free energy of going from the crystal structure conformation of the apo S1S2 (~**2**) to **4** is −8.8 kcal/mol, and the free energy of going from **1** to **4** is −11.7 kcal/mol.

An experimental estimate for the overall equilibrium dissociation constant ($K_D$) for glutamate binding to S1S2 is 0.48 μM (Abele et al., 2000), which corresponds to about −8.7 kcal/mol (from $\Delta G = RT\ln K_D$, where $R$ is the gas constant and $T$ is temperature). Our glutamate-bound S1S2 computations consider, however, only the conformational free energy of the system in which glutamate is already bound to S1S2; they do not consider the process of taking the ligand from bulk solvent and docking it into the cleft. This docking step must be taken into account before computed results can be compared with an overall $K_D$ (Woo and Roux, 2005).

The crystal structures of glutamate- and AMPA-bound S1S2 show that the peptide bond between D651 and S652 can adopt conformations that allow two additional hydrogen bonds to form between Lobes 1 and 2 that are not seen in our simulations (Armstrong and Gouaux, 2000). This alternate conformation is seen in chain C, but not chain A, of the glutamate-bound S1S2 crystal structure. The formation of these additional hydrogen bonds is expected to increase the stability of the closed cleft relative to our computed values. Computations that explicitly consider the "flipping" of the peptide bond between D651 and S652 would have to be carried out in order to evaluate how much additional stability is obtained.

Over the course of all simulations, the average root-mean-square deviation (rmsd) measured separately in Lobe 1 (calculated at α-carbon atoms of residues 394–495 and 732–771) and Lobe 2 (calculated at α-carbon atoms of residues 500–728) with respect to the corresponding crystal structure (chain A) was ~1 Å, consistent with the magnitude of thermal fluctuation. This observation also indicates that distributions in $\xi_1$ and $\xi_2$ reflect fluctuations in the relative orientation of the two lobes rather than intra-lobe distortions. The broad free energy basin of the apo S1S2 and the narrow basin of the glutamate-bound S1S2 are consistent with previous MD simulations described by Arinaminpathy et al. (2006), which showed more conformational fluctuation in the apo protein, in both open

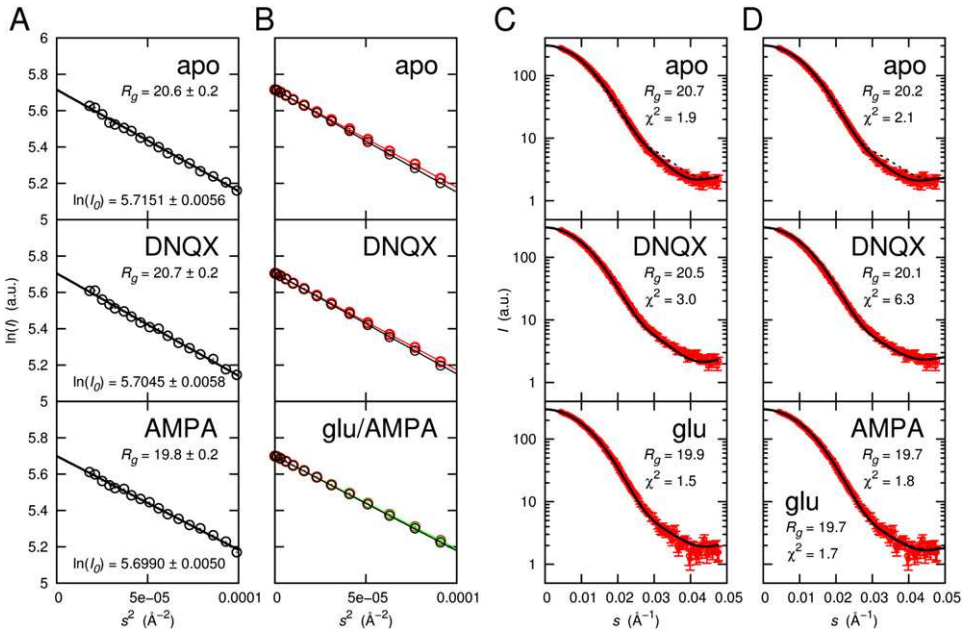


**Figure 3. Small-Angle X-Ray Scattering**

(A) $R_g$ values for the apo, DNQX-, and AMPA-bound S1S2 were obtained by fitting experimental SAXS profiles (Madden et al., 2005) to the Guinier law in the range $2\pi sR_g < 1.3$.

(B) $R_g$ values obtained by fitting calculated scattering profiles to the Guinier law in the same range.

$R_g$ values are shown in (C) and (D). Ensemble average scattering profiles from simulations (black) are compared with scattering profiles calculated from X-ray crystal structures (PDB ID: 1FTO [apo, red], 1FTL [DNQX, red], 1FTM [AMPA, red], 1FTJ [glu, green]). Calculated scattering are shown as circles, and Guinier fits are shown as lines. The calculated curves were scaled such that $I_0$ matched those obtained for the experimental curves. The AMPA and glu crystal results are nearly indistinguishable.

(C) Comparison of ensemble average scattering profiles from simulations (black lines) with experimental profiles (red circles). Error bars in the experimental data indicate standard deviation. $R_g$ for the calculated scattering profiles and $\chi^2$ (evaluated by using all experimental data) are shown. The dashed line in the apo panel is the scattering profile that results when binding cleft waters are omitted from the scattering calculations. In the bottom panel, the calculated scattering profile for the glutamate-bound S1S2 is compared with experimental data for AMPA-bound S1S2.

(D) Comparison of scattering profiles calculated from X-ray crystal structures (black lines) with experimental profiles (red circles). Crystallographically unresolved protein termini and side chains were built into the models since they contribute to X-ray scattering. $R_g$ for the calculated scattering profiles and $\chi^2$ (evaluated by using all experimental data) are shown. As in (C), the dashed line in the apo panel is the scattering profile that results when binding cleft waters are omitted from the scattering calculations. In the bottom panel, experimental data for the AMPA-bound S1S2 are compared with calculated scattering profiles for both AMPA-bound (solid line) and glutamate-bound (dashed line) S1S2.

and closed states, compared with the glutamate-bound protein.

## Comparison with Experiments Probing S1S2 in Solution

The present simulations sample and explore conformations that are not limited to the neighborhood of available X-ray crystal structures. In particular, low-energy conformations—~10° more open than seen in crystal structures of the apo GluR2—are accessible according to the computations. Thus, it is important to validate, as much as possible, the S1S2 free energy landscapes and conformations resulting from the simulations by using all available experimental information.

### *Small-Angle X-Ray Scattering Analysis*

Small-angle X-ray scattering (SAXS) provides partial, but important, clues to S1S2 conformations in solution that are helpful to ascertain the accuracy of the simulations. To validate the S1S2 free energy landscapes and conformations resulting from the simulations, SAXS curves were calculated from the simulations and compared with experimental results. Figure 3A shows the radii of gyration, $R_g$, and forward scattering, $I_0$, for the apo, DNQX-, and AMPA-bound S1S2, as determined by fitting the SAXS data of Madden et al. (2005) to the Guinier law in the range $2\pi sR_g < 1.3$, where $s$ is the magnitude of the scattering vector in reciprocal space (see Experimental Procedures).

Ensemble average scattering profiles were calculated for each protein system by using snapshots taken from simulation trajectories. Experimental SAXS data for glutamate-bound S1S2 were not available, so calculated scattering profiles for the glutamate-bound S1S2 were compared with SAXS data for AMPA-bound S1S2, which seems to be a reasonable comparison. For each system, two snapshots were selected every 0.1 Å along $\xi_{12}$ in the following ranges: 8.2 Å $\leq \xi_{12} \leq$ 24.0 Å for the apo S1S2, 8.6 Å $\leq \xi_{12} \leq$ 24.2 Å for the DNQX-bound S1S2, and 8.1 Å $\leq \xi_{12} \leq$ 24.3 Å for the glutamate-bound S1S2. The two snapshots were selected from different time frames, one from 800 ps $< t \leq$ 900 ps and the other

from 900 ps $< t \leq$ 1000 ps of the respective umbrella window trajectories. Since multiple snapshots can map to a single value of $\xi_{12}$, snapshots were taken from the minimum $W$ ($\xi_1$,$\xi_2$) corresponding to each $\xi_{12}$. A scattering curve $I_{sol}(s)$ was calculated for each snapshot by using the program CRYSOL (Svergun et al., 1995) (see Experimental Procedures), and ensemble average scattering profiles $\langle I_{sol}(\boldsymbol{s})\rangle$ were calculated by using Equation 7. Figure 3C shows a comparison between the calculated $\langle I_{sol}(\boldsymbol{s})\rangle$ and experimental scattering profiles, including the calculated $R_g$ (determined by using the Guinier approximation) and the $\chi^2$ value, which is a measure of the quality of agreement. The calculated and experimental profiles agree very well. All water molecules and $Na^+$ and $Cl^-$ ions were removed from the DNQX- and glutamate-bound protein system snapshots before $I_{sol}(s)$ was calculated. For the apo protein system snapshots, however, a cluster of water molecules within the ligand-binding cleft near the charged guanidinium group of R485 (~25 waters for conformations where $\xi_{12}$ = 12 Å) was included in the calculation of $I_{sol}(s)$. All other water molecules and all $Na^+$ and $Cl^-$ ions were removed. This water cluster may contribute to stabilizing the apo S1S2 in an open-cleft conformation. Inclusion of the water cluster in the apo S1S2 markedly improved agreement between the calculated and experimental scattering profiles (Figure 3C, apo). Inclusion of additional water molecules outside the ligand-binding cleft did not improve agreement. The continuum model of the hydration shell used in CRYSOL may not adequately account for tightly bound water molecules within the binding cleft of the apo S1S2, thus necessitating the explicit inclusion of these waters. The DNQX and glutamate ligands both bind to the guanidinium group of R485, interfering with its interaction with solvent; thus, water molecules were not explicitly included in these snapshots.

Scattering profiles were also calculated from X-ray crystal structures of the apo, DNQX-, glutamate-, and AMPA-bound S1S2 (all chain A) and were compared with the experimental profiles (Figure 3D). Crystallographically unresolved protein termini and side chains were built into the models since they contribute to X-ray scattering (see Experimental Procedures). As with the simulated snapshots, inclusion of a water cluster (25 molecules) in the ligand-binding cleft of the apo S1S2 markedly improved agreement between the calculated and experimental profiles.

For the apo and DNQX-bound S1S2, the calculated ensemble average profiles from the simulations agree significantly better with the experimental profiles than the calculated profiles from the crystal structures. The differences in agreement are seen primarily in $R_g$ for the apo S1S2 and in both $R_g$ and $\chi^2$ for the DNQX-bound S1S2 (Figure 3). In the original analysis of the SAXS data in which only crystal structures were used for the atomic models, it was suggested that the apo S1S2 primarily samples conformations intermediate to the DNQX- and AMPA-bound S1S2 structures (Madden et al., 2005). Our analysis, on the other hand, suggests that the apo S1S2 is not limited to this range of conformations, but rather extensively populates more open conformations. For the glutamate-/AMPA-bound S1S2, the calculated ensemble average profile from the simulations and the calculated profiles from the crystal structures agree similarly with the experimental profile (the calculated ensemble average profile agrees slightly better, as seen in the $\chi^2$ value). The similarity in these calculated profiles is not surprising given that the narrow and deep global free energy minimum for the glutamate-bound S1S2 is positioned close to the crystal structure conformations of both the glutamate- and AMPA-bound S1S2. Fits to the Guinier law in the determination of $R_g$ for the calculated profiles are shown in Figure 3B. The experimental scattering profiles reflect ensembles of conformational states, and the relative populations of these conformational states appear to be captured in the computed free energy landscapes.

### *Fluorescence Resonance Energy Transfer*

Recent fluorescence resonance energy transfer (FRET) experiments, aimed at characterizing the largest molecular motions in S1S2, have measured the distance between fluorophores attached to residue 394 in Lobe 1 and residue 652 in Lobe 2 in the apo and various ligand-bound forms (Ramanoudjame et al., 2006). It was concluded that, in solution, S1S2 exhibits a smaller degree of cleft closure in going from the apo to agonist-bound forms than indicated by the crystal structures. Such a small movement upon cleft closure might be taken as an indication that the apo state in solution is opened to a lesser extent than observed in the crystal structure. This does not, however, seem plausible. Analysis of steric clashes suggests that, unless the apo cleft opens to at least the extent observed in the crystal structure of the apo S1S2, a ligand will have a very difficult time maneuvering into the partially open cleft to reach the binding site. In fact, the present computations suggest rather the opposite—that the apo state could sometimes be even more open than observed in the crystal structure, a finding that is consistent with SAXS data (see above). Alternatively, the small movement detected by FRET could be interpreted as an indication that AMPA- and glutamate-bound S1S2 are more open than indicated by the crystal structures. The free energy landscape of glutamate-bound S1S2 calculated in solution, however, indicates that the complex resides at the bottom of a deep well, consistent with the crystal structure, suggesting that large excursions to more opened states are unlikely. A third possibility is that the small movement detected by FRET might be inherent to the method. Because the rate of energy transfer varies as the inverse sixth-power of the donor-acceptor distance according to Förster's theory, short distances tend to be weighted more heavily in FRET-based distance measurements (Stryer and Haugland, 1967), hence yielding an appearance of small distances for both the apo and agonist-bound states of S1S2. To draw definitive conclusions, simulations of S1S2 explicitly including the attached fluorophores would have to be performed in order to reasonably compare computed ensemble average distances with the experimental measurements.

 

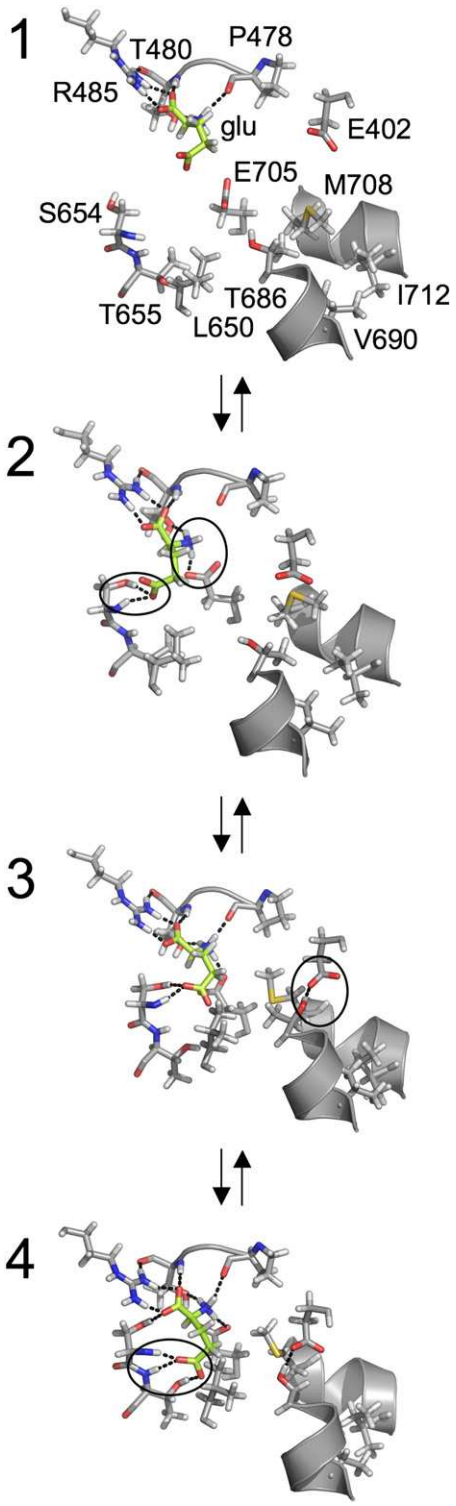


**Figure 4. Ligand-Binding Cleft Interactions Corresponding to Different States of S1S2 Opening or Closing in the Presence of a Glutamate Ligand**

The snapshots, taken from MD trajectories, correspond to the conformational states labeled **1**–**4** in Figure 2A (glu). Carbon atoms of the glutamate ligand are colored green. Dotted lines indicate hydrogen-bonding interactions. Water molecules are not shown in order to focus on direct protein-ligand and protein-protein interactions. Key interactions associated with each conformational state are circled. The hydrogen bonding of the ligand $\alpha$-amino group with the S654 backbone/side chain and the ligand $\gamma$-carboxylate group with the E705 side chain characterize the transition from **1** to **2**. The hydrogen bonding of the E402 side chain with the T686 side chain characterize the transition from **2** to **3**. A shift of the ligand $\gamma$-carboxylate group's hydrogen-bonding partners from the S654 backbone/side chain to both the S654 backbone and the T655 backbone/side chain characterize the transition from **3** to **4**.

## State-Dependent Interactions within the Ligand-Binding Cleft

Specific protein-ligand and intraprotein interactions within the S1S2 ligand-binding cleft give rise to features in the free energy landscape of S1S2 with a bound glutamate (Figures 2 and 4). State **1** in Figure 2A (glu) corresponds to a glutamate-bound open form of S1S2. In the absence of ligand, this is an energetically easily accessible conformation of the apo S1S2 that is more open than has been observed in X-ray crystal structures (Figure 2A, apo). With a bound ligand, such an open form of S1S2 has the character of an unstable "virtual" state, which should ultimately relax to the closed form. In such an open state, the glutamate ligand interacts only with Lobe 1. This occurs spontaneously during the umbrella sampling MD simulations. This state might correspond to the "dock" step of the "dock-lock" mechanism of glutamate receptor ligand-binding suggested previously on the basis of functional and kinetics studies (Abele et al., 2000; Cheng et al., 2005) in which the ligand is bound exclusively to Lobe 1 prior to complete cleft closure. In state **1**, the binding cleft is open wide enough for the glutamate ligand to easily access its crystallographically observed binding partners in Lobe 1 (P478, T480, and R485) without necessarily interacting with residues in Lobe 2. Comparison with the apo simulations indicates that binding of the ligand to R485 displaces water molecules clustered around the guanidinium group of that residue. Thus, if occupation by water molecules stabilizes the cleft in open conformations in the absence of ligand, then the displacement of these water molecules would be the first step in driving cleft closure.

Further cleft closure is driven by the formation of additional hydrogen bonds between the ligand and Lobe 2, while the former remains strongly bound to Lobe 1. For instance, the transition from state **1** to state **2**, which is near the crystal structure conformation of the apo S1S2, is characterized by the formation of hydrogen bonds between the glutamate ligand $\alpha$-amino group with the S654 backbone/side chain and the ligand $\gamma$-carboxylate group with the E705 side chain. In the apo S1S2 crystal structure, the side chains of E705 and K730 interact. The disruption of this interaction to form the hydrogen bond between the glutamate ligand and E705 is consistent with the suggestion of a conformational switch involving E705 and K730 (Armstrong and Gouaux, 2000; Armstrong et al., 2003; Mayer et al., 2006). In going from **1** to **2**, the ligand-bound complex is further stabilized by 5.1 kcal/mol.

The transition from **2** to **3**, which yields an additional stabilization free energy of 0.2 kcal/mol, is characterized by the formation of a hydrogen bond between the side chains of E402 and T686. The association of these two residues is captured in $\xi_2$. Protein-ligand interactions remain similar to those in **2**. A 0.6 kcal/mol barrier separates **2** and **3**. Analysis indicates that this small free energy barrier corresponds to the cost of aligning E402 and T686 such that steric hindrance is avoided and hydrogen bond formation is allowed. This interaction is further examined in the next section.

Finally, 6.4 kcal/mol is gained in the transition from **3** to **4**, which results in a fully closed S1S2. This final transition is characterized by a shift in the glutamate ligand $\gamma$-carboxylate group's hydrogen-bonding partners from the S654 backbone/side chain to both the S654 backbone and the T655 backbone/side chain. This shift in hydrogen bonding is captured in $\xi_1$. In this fully closed, or "locked," conformation, the ligand-binding pocket is fully encapsulated by the protein (i.e., the ligand cannot be seen from outside the protein in a molecular surface representation of the complex). S1S2 opening and the release of a bound glutamate ligand from **4** would be accomplished via the hydrogen-bonding events occurring in reverse order. It has been suggested, however, that concerted movement of a helix in Lobe 2 may allow for ligand dissociation without S1S2 opening (McFeeters and Oswald, 2002). Overall, a total stabilization of 9–12 kcal/mol is gained during the transformation from the open to the closed state in the presence of a bound ligand: 8.8 kcal/mol is gained in going from the crystal structure conformation of the apo S1S2 (~**2**) to **4**, or 11.7 kcal/mol is gained in going from **1** to **4**. This is the free energy that is available upon ligand binding to move the segments in Lobe 2 connected to the gate of the GluR2 transmembrane domain, leading to channel opening.

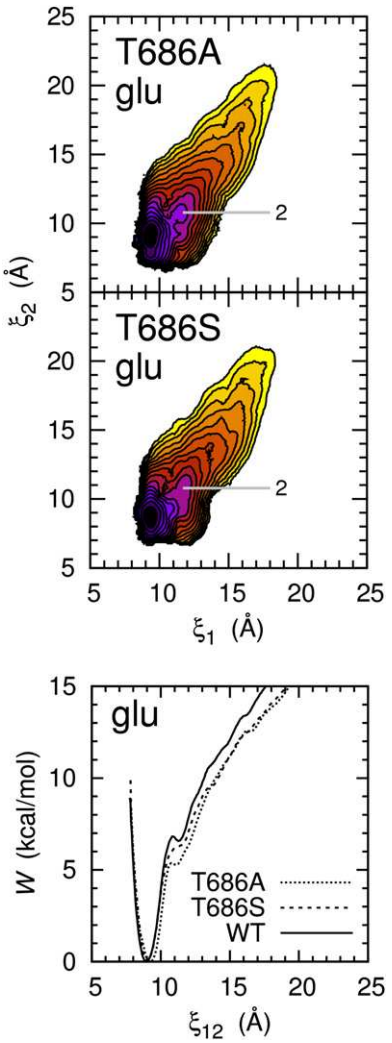


**Figure 5. The Free Energy Landscapes for Conformational Changes in the T686A and T686S Glutamate-Bound S1S2**

In the 2D PMF maps (top two panels), each color contour corresponds to 1 kcal/mol. Conformational state **2** from Figure 2A (glu) is labeled. In the 1D PMF plot (bottom panel), the PMF along the reduced coordinate $\xi_{12}$ is shown. The WT plot is the same as that shown in Figure 2B (glu).

## T686A and T686S Mutants

In order to further probe details of conformational transitions in S1S2, we computed free energy landscapes for two mutants of the glutamate-bound S1S2, T686A and T686S. In comparing the free energy landscapes of the mutants in Figure 5 with the free energy landscape of the wild-type (WT) glutamate-bound S1S2 in Figure 2A (glu), the free energy barrier separating state **2** from the edge of the basin in the WT free energy landscape (i.e., state **3** in Figure 2A, glu) is seen to largely vanish in the mutant free energy landscapes. During S1S2 closure, steric hindrance is reduced between residues 402 and 686 in both T686A and T686S compared with WT. During S1S2 opening, no hydrogen bonds are broken between these two residues in T686A. A hydrogen bond is broken, however, in the T686S protein, but S686 appears to be more mobile around the $\chi_1$ bond than T686 (T686 is restricted to conformations in which the side chain methyl group can occupy the hydrophobic groove formed by L650, V690, L704, M708, and I712) and may offer a less stable hydrogen bond than T686. The free energy required to go from the fully closed state to state **2** is 7.7 kcal/mol for T686A and 8.3 kcal/mol for T686S.

In the 1D PMF plots for the T686A, T686S, and WT S1S2 (Figure 5, bottom panel), the free energies associated with conformations in which $\xi_{12} > 9.0$ Å follow the order T686A < T686S < WT. Transitions between state **2** and more fully closed states would occur more easily in the mutant proteins than in the WT protein. Though a comparison is difficult, these results are consistent with those of Robert et al. (2005), who observed a reduction in the apparent affinity and efficacy of glutamate in T686A and T686S mutants of GluR2, and suggest that the T686 mutations destabilize cleft closure, which increases the rate of agonist dissociation. These mutations were also observed to speed recovery from desensitization.

 

## Conclusion

All-atom MD simulations with explicit solvent, in conjunction with an umbrella sampling strategy, were used to compute free energy landscapes that govern conformational changes in GluR2 S1S2 driving receptor activation. We find that the apo S1S2 can easily adopt conformations in which the binding cleft is more open than has been observed in X-ray crystal structures. Further analysis indicates that the conformations sampled by the simulations are compatible with experimental SAXS data. It is possible that crystal lattice contacts may contribute to stabilizing the apo S1S2 in the crystallographically observed conformation, while the apo S1S2 explores more open conformations in solution. In addition, the analysis of SAXS data suggests that a dense cluster of water molecules may form in the apo cleft near the guanidinium group of R485. This cluster of water may stabilize the cleft in an open conformation. Ligand binding to R485 would disrupt the formation of this cluster, facilitating cleft closure. The free energy landscapes for the WT and mutant S1S2 reveal key interactions in the ligand-binding cleft associated with different states of cleft closure and support the importance of the E402-T686 interaction (Robert et al., 2005) in stabilizing a closed cleft. A free energy of 9–12 kcal/mol becomes available upon glutamate binding for driving the conformational changes in S1S2 associated with opening the GluR2 transmembrane ion channel: this free energy is 9 kcal/mol if the ligand docks in the cleft while the latter is in the apo S1S2 crystal structure conformation or 12 kcal/mol if the ligand docks in a more open cleft.

## EXPERIMENTAL PROCEDURES

### Atomic Models

The atomic models for the apo, DNQX-bound, glutamate-bound, and AMPA-bound GluR2 S1S2 monomers were constructed from the following Protein Data Bank (PDB) X-ray crystal structures: 1FTO (apo), 1FTL (DNQX), 1FTJ (glu), and 1FTM (AMPA) (Armstrong and Gouaux, 2000). Each of these PDB entries contains multiple copies of S1S2 within the asymmetric unit. Our models were all constructed from chain A (the other chains share similar conformations). The choice of chain A was arbitrary; given the small conformational differences among chains in each crystal structure and the presence of thermal fluctuations in the MD simulations, the present results are not expected to be sensitive to small differences in the starting conditions. The model of the AMPA-bound S1S2 was used only in calculating SAXS profiles. The terminal amino acids and several side chains are unresolved in the crystal structures, so they were built into the models. Missing amino acids were built by using the loop-modeling routine of the program MODELER (Fiser and Sali, 2003). Missing side chains were built by using the program SCWRL (Canutescu et al., 2003), which searches for optimal rotamers with a backbone-dependent library of side chains. T686A and T686S mutations of the glutamate-bound S1S2 model were also generated by using SCWRL. Crystallographic waters observed in the ligand-binding cleft were included in our models.

DNQX was parameterized for the CHARMM PARAM27 all-atom potential-energy function for proteins (MacKerell et al., 1998). In brief, this procedure involved (1) charge fitting a geometry-optimized molecule to quantum mechanical (QM) electrostatic potential maps (by using the Gaussian 03 program [Frisch et al., 2004] for quantum chemical calculations and the FITCHARGE module of CHARMM [Anisimov et al., 2005; Bayly et al., 1993] for charge fitting), (2) optimizing force constants via the reproduction of vibrational frequencies and potential-energy distributions from QM calculations (by using the Gaussian 03 program, the MOLVIB module of CHARMM, and a novel genetic algorithm to search for force constants), and (3) optimizing dihedral parameters associated with rotatable bonds via the reproduction of dihedral potential-energy surfaces from QM calculations.

### PMF from Umbrella Sampling Simulations

The PMF corresponds to the average reversible thermodynamic work function $W(\xi)$ done by the mean force $\langle F(\xi)\rangle$ along the chosen order parameter $\xi$, i.e.,

$$W(\xi) = W(\xi^*) - \int d\xi \langle F(\xi)\rangle = W(\xi^*) - k_B T \ln\left[\frac{\langle \rho(\xi)\rangle}{\langle \rho(\xi^*)\rangle}\right], \qquad (1)$$

where $\langle \rho(\xi)\rangle$ is the average distribution function, $\xi^*$ and $W(\xi^*)$ are arbitrary constants, $k_B$ is Boltzmann's constant, and $T$ is temperature (Roux and Schulten, 2004).

A 2D order parameter, $(\xi_1,\xi_2)$, is used to describe the opening or closing of S1S2 (Figure 1). $\xi_1$ describes the distance between the center-of-mass (COM) of residues 479–481 in Lobe 1 and residues 654–655 in Lobe 2. $\xi_2$ describes the distance between the COM of residues 401–403 in Lobe 1 and residues 686–687 in Lobe 2.

Starting coordinates for the umbrella sampling windows were obtained by using a targeted (biased-potential) MD procedure to generate conformations positioned in 1.0 Å increments along $\xi_1$ from 8.0 to 22.0 Å and 1.0 Å increments along $\xi_2$ from 6.0 to 26.0 Å. Starting coordinates for each window of both the apo and glutamate-bound S1S2 simulations were generated from the crystal structure of the glutamate-bound S1S2 (the glutamate ligand was removed to yield apo S1S2 coordinates). Starting coordinates for each window of the DNQX-bound protein simulations were generated from the crystal structure of the DNQX-bound S1S2. During the generation of starting conformations, (1) rmsd restraints were applied separately to each lobe of S1S2 (Lobe 1: residues 394–495 and 732–771; Lobe 2: residues 500–728) with respect to the crystal structure such that the rmsd for each lobe <1 Å, and (2) the DNQX and glutamate ligands were restrained to remain bound to R485, as observed in the crystal structures, to be consistent with the "dock-lock" mechanism of GluR ligand binding (Abele et al., 2000; Cheng et al., 2005), in which the ligand is suggested to bind to Lobe 1 prior to complete cleft closure.

All simulations were performed by using the program CHARMM (Brooks et al., 1983). The all-atom potential-energy function PARAM27 for proteins (MacKerell et al., 1998) and the TIP3P potential energy function for water (Jorgensen et al., 1983) were used. The total number of atoms in each simulation system is ~47,000. To electrically neutralize each system, 37 $Na^+$ and either 42 $Cl^-$ (for the apo and DNQX-bound protein systems) or 41 $Cl^-$ (for the glutamate-bound protein system) ions were added in the bulk solution to yield 150 mM NaCl. Periodic boundary conditions were used with an orthorhombic cell with approximate dimensions 97 Å × 77 Å × 65 Å. Electrostatic interactions were computed by using the particle mesh Ewald (PME) algorithm (Essmann et al., 1995), and short-range, nonbonded interactions were truncated at 10 Å. The SHAKE algorithm (Ryckaert et al., 1977) was used to constrain bond lengths involving hydrogen atoms. A time step of 2 fs was used. The initial protein configuration of each system was first relaxed with Langevin dynamics in the presence of harmonic restraints at constant volume for 200 ps to avoid spurious disruption of the protein structure. The cell dimensions were subsequently allowed to vary in accordance with a constant pressure (1 atm) and temperature (300 K) thermodynamic ensemble (Feller et al., 1995).

For the umbrella sampling PMF calculations, 200 independent simulations with biasing harmonic potential functions of 2.0 kcal/mol/Å$^2$ centered on the $(\xi_1,\xi_2)$ positions of the starting coordinates described above were generated. The COM biasing potentials were implemented by using the MMFP module of CHARMM (Brooks et al., 1983). The entire simulation time included in the PMF calculations is 200 ns (1 ns of

trajectory generation per window) for each of the apo, DNQX-, and glutamate-bound WT S1S2 systems. The entire simulation time is 180 ns (0.9 ns per window) for the glutamate-bound T686A and T686S systems. The distribution functions in $(\xi_1,\xi_2)$ from all windows were unbiased and recombined by using the weighted histogram analysis method (WHAM) (Kumar et al., 1992; Souaille and Roux, 2001) to calculate the PMF $W(\xi_1,\xi_2)$. $W(\xi_1,\xi_2)$ was also projected onto the reduced coordinate $\xi_{12} = (\xi_1 + \xi_2)/2$ to give a 1D PMF $W(\xi_{12})$.

Cleft opening or closing described in terms of rotation around an effective hinge connecting Lobes 1 and 2 was calculated by using the script HINGEFIND (Wriggers and Schulten, 1997) implemented in the program VMD (Humphrey et al., 1996).

### Small-Angle X-Ray Scattering Analysis

The scattering intensity profile for a molecule in vacuum is given by the Debye equation (Debye, 1915):

$$I_{\mathrm{vac}}(s) = \left\langle |F(\mathbf{s})|^2 \right\rangle_{\Omega} = \sum_{j=1}^{N}\sum_{k=1}^{N} f_j(s) f_k(s) \frac{\sin(2\pi s r_{jk})}{2\pi s r_{jk}}, \quad (2)$$

where $F(\mathbf{s})$ is the molecular structure factor in vacuum,

$$F(\mathbf{s}) = \sum_{j=1}^{N} f_j(\mathbf{s}) e^{i\mathbf{s}\mathbf{r}_j}. \quad (3)$$

In Equations 2 and 3, $\mathbf{s}$ is the scattering vector in reciprocal space ($|\mathbf{s}| = s = (2/\lambda)\sin\theta$, where $\lambda$ is the X-ray wavelength and $\theta$ is half the scattering angle), $f_j(\mathbf{s})$ is the vacuum atomic scattering factor of the $j^{\mathrm{th}}$ atom, $N$ is the number of atoms in the molecule, $\mathbf{r}_j$ represents the coordinates of the $j^{\mathrm{th}}$ atom, $\mathbf{r}_{jk}$ is the distance between atoms $j$ and $k$, and $\langle\rangle_{\Omega}$ denotes a spherical average in reciprocal space. The scattering profile can also be written as:

$$I_{\mathrm{vac}}(s) = \int_0^{\infty} P(r) \frac{\sin(2\pi s r)}{2\pi s r} dr, \quad (4)$$

where $P(r) = \sum_{j=1}^{N}\sum_{k=1}^{N} f_j(s) f_k(s) \delta(r - r_{jk})$ is the weighted interatomic distance distribution function.

In evaluating the scattering profile for a molecule in solution, the solvent scattering must be taken into account. In this case,

$$I_{\mathrm{sol}}(s) = \left\langle |F(\mathbf{s}) - G(\mathbf{s})|^2 \right\rangle_{\Omega}, \quad (5)$$

where $G(\mathbf{s})$ is the solvent scattering amplitude and $F(\mathbf{s}) - G(\mathbf{s})$ is the total excess scattering amplitude. The solvent scattering amplitude may be expressed as (Svergun et al., 1995):

$$G(\mathbf{s}) = \rho_0 A(\mathbf{s}) - (\rho_b - \rho_0) B(\mathbf{s}), \quad (6)$$

where $\rho_0$ is the average bulk solvent scattering density, $A(\mathbf{s})$ is the scattering amplitude from the excluded volume (i.e., the volume occupied by the solute), $\rho_b$ is the scattering density of the hydration shell surrounding the solute, and $B(\mathbf{s})$ is the scattering amplitude from the hydration shell.

Ensemble average scattering profiles $\langle I_{\mathrm{sol}}(s)\rangle$ using snapshots $j$ taken from simulation trajectories are calculated as follows:

$$\langle I_{\mathrm{sol}}(s)\rangle = \frac{\sum_j I_{\mathrm{sol},j}(s) e^{-W_j(\xi_1,\xi_2)/k_{\mathrm{B}}T}}{\sum_j e^{-W_j(\xi_1,\xi_2)/k_{\mathrm{B}}T}}, \quad (7)$$

where $k_{\mathrm{B}}$ is Boltzmann's constant and $T$ is temperature. $I_{\mathrm{sol},j}(s)$ were calculated by using the program CRYSOL (Svergun et al., 1995), which uses a continuum model of the hydration shell modeled to be 3 Å thick to simulate the first hydration layer. In the CRYSOL fitting process, $\rho_0$ was fixed at 0.334 eÅ$^{-3}$. $\rho_b$ ranged from 0.344 to 0.351 eÅ$^{-3}$, which falls between values calculated for staphylococcal nuclease (Smolin and Winter, 2004) and observed for lysozyme, *Escherichia coli* thioredoxin reductase, and protein R1 of *E. coli* ribonucleotide reductase by using small-angle X-ray and neutron scattering techniques (Svergun et al., 1998). The excluded volume for the protein snapshots ranged from 38,500 to 41,400 Å$^3$, consistent with values obtained by using the rolling ball algorithm described by Richards (Richards, 1977; Voss et al., 2006). SAXS data for the GluR2 S1S2 in the apo, DNQX-bound, and AMPA-bound forms were kindly provided by D.R. Madden and P. Vachette (Madden et al., 2005).

The radii of gyration, $R_{\mathrm{g}}$, were determined from the Guinier approximation (Guinier, 1939), $I(s) \approx I_0 \exp[-(2\pi s)^2 R_{\mathrm{g}}^2/3]$, in the range $2\pi s R_{\mathrm{g}} < 1.3$, where $I_0$ is the forward scattering. The intercept of the Guinier plot ($\ln[I(s)]$ versus $(2\pi s)^2$) gives $I_0$, and the slope yields $R_{\mathrm{g}}$. The quality of agreement between the calculated and experimental scattering profiles is evaluated by using the $\chi^2$ function,

$$\chi^2 = \frac{1}{N-1}\sum_{m=1}^{N}\left(\frac{I_{\mathrm{exp}}(s_m) - I_{\mathrm{calc}}(s_m)}{\sigma(s_m)}\right)^2, \quad (8)$$

where $N$ is the number of experimental data points, $I_{\mathrm{exp}}(s_i)$ and $I_{\mathrm{calc}}(s_i)$ are the experimental and calculated scattering profiles, respectively, and $\sigma(s_i)$ is the experimental standard deviation. Interpolation in the calculated profiles was performed by using a cubic spline.

## ACKNOWLEDGMENTS

We thank N.K. Banavali, Y. Deng, J.D. Faraldo-Gómez, E. Harder, V. Jogini, G. Lamoureux, S.Y. Noskov, A.C. Pan, J.L. Robertson, and D. Sezer for helpful discussion. We thank D.R. Madden and P. Vachette for kindly providing the GluR2 S1S2 SAXS data. This work was partially supported by National Institutes of Health Grants GM 62342 and CA 93577. Computational support from the National Center for Supercomputing Applications (NCSA) and the Pittsburgh Supercomputing Center (PSC) obtained through the National Resource Allocations Committee (NRAC) was used for the calculations.

Received: June 4, 2007
Revised: July 27, 2007
Accepted: July 31, 2007
Published: October 16, 2007

## REFERENCES

Abele, R., Keinänen, K., and Madden, D.R. (2000). Agonist-induced isomerization in a glutamate receptor ligand-binding domain. A kinetic and mutagenetic analysis. J. Biol. Chem. *275*, 21355–21363.

Ahmed, A.H., Loh, A.P., Jane, D.E., and Oswald, R.E. (2007). Dynamics of the S1S2 glutamate binding domain of GluR2 measured using 19F NMR spectroscopy. J. Biol. Chem. *282*, 12773–12784.

Anisimov, V.M., Lamoureux, G., Vorobyov, I.V., Huang, N., Roux, B., and MacKerell, A.D., Jr. (2005). Determination of electrostatic parameters for a polarizable force field based on the classical drude oscillator. J. Chem. Theo. Comp. *1*, 153–168.

Arinaminpathy, Y., Sansom, M.S., and Biggin, P.C. (2006). Binding site flexibility: molecular simulation of partial and full agonists within a glutamate receptor. Mol. Pharmacol. *69*, 11–18.

Armstrong, N., and Gouaux, E. (2000). Mechanisms for activation and antagonism of an AMPA-sensitive glutamate receptor: crystal structures of the GluR2 ligand binding core. Neuron *28*, 165–181.

Armstrong, N., Sun, Y., Chen, G.Q., and Gouaux, E. (1998). Structure of a glutamate-receptor ligand-binding core in complex with kainate. Nature *395*, 913–917.

Armstrong, N., Mayer, M., and Gouaux, E. (2003). Tuning activation of the AMPA-sensitive GluR2 ion channel by genetic adjustment of

 

agonist-induced conformational changes. Proc. Natl. Acad. Sci. USA *100*, 5736–5741.

Armstrong, N., Jasti, J., Beich-Frandsen, M., and Gouaux, E. (2006). Measurement of conformational changes accompanying desensitization in an ionotropic glutamate receptor. Cell *127*, 85–97.

Asztely, F., and Gustafsson, B. (1996). Ionotropic glutamate receptors. Their possible role in the expression of hippocampal synaptic plasticity. Mol. Neurobiol. *12*, 1–11.

Ayalon, G., and Stern-Bach, Y. (2001). Functional assembly of AMPA and kainate receptors is mediated by several discrete protein-protein interactions. Neuron *31*, 103–113.

Banavali, N.K., and Roux, B. (2005). The N-terminal end of the catalytic domain of SRC kinase Hck is a conformational switch implicated in long-range allosteric regulation. Structure *13*, 1715–1723.

Bayly, C.I., Cieplak, P., Cornell, W.D., and Kollman, P.A. (1993). A well-behaved electrostatic potential based method using charge restraints for deriving atomic charges: the RESP model. J. Phys. Chem. *97*, 10269–10280.

Bräuner-Osborne, H., Egebjerg, J., Nielsen, E.Ø., Madsen, U., and Krogsgaard-Larsen, P. (2000). Ligands for glutamate receptors: design and therapeutic prospects. J. Med. Chem. *43*, 2609–2645.

Brooks, B.R., Bruccoleri, R.E., Olafson, B.D., States, D.J., Swaminathan, S., and Karplus, M. (1983). CHARMM: a program for macromolecular energy, minimization, and dynamics calculations. J. Comput. Chem. *4*, 187–217.

Canutescu, A.A., Shelenkov, A.A., and Dunbrack, R.L., Jr. (2003). A graph-theory algorithm for rapid protein side-chain prediction. Protein Sci. *12*, 2001–2014.

Cheng, Q., Du, M., Ramanoudjame, G., and Jayaraman, V. (2005). Evolution of glutamate interactions during binding to a glutamate receptor. Nat. Chem. Biol. *1*, 329–332.

Cull-Candy, S., Kelly, L., and Farrant, M. (2006). Regulation of $Ca^{2+}$-permeable AMPA receptors: synaptic plasticity and beyond. Curr. Opin. Neurobiol. *16*, 288–297.

Debye, P. (1915). Zerstreuung von Röntgenstrahlen. Ann. Physiol. (Leipzig) *46*, 809–823.

Dingledine, R., Borges, K., Bowie, D., and Traynelis, S.F. (1999). The glutamate receptor ion channels. Pharmacol. Rev. *51*, 7–61.

Essmann, U., Perera, L., Berkowitz, M.L., Darden, T., Lee, H., and Pedersen, L.G. (1995). A smooth particle mesh Ewald method. J. Chem. Physiol. *103*, 8577–8593.

Feller, S.E., Zhang, Y., Pastor, R.W., and Brooks, B.R. (1995). Constant pressure molecular dynamics simulation: the Langevin piston method. J. Chem. Physiol. *103*, 4613–4621.

Fiser, A., and Sali, A. (2003). ModLoop: automated modeling of loops in protein structures. Bioinformatics *19*, 2500–2501.

Frisch, M.J., Trucks, G.W., Schlegel, H.B., Scuseria, G.E., Robb, M.A., Cheeseman, J.R., Montgomery, J.A., Jr., Vreven, T., Kudin, K.N., Burant, J.C., et al. (2004). Gaussian 03, Revision C.02 (http://www.gaussian.com).

Guinier, A. (1939). La diffraction des rayons X aux très faibles angles: applications à l'etude des phénomènes ultra-microscopiques. Ann. Physiol. (Paris) *12*, 161–236.

Hollmann, M., and Heinemann, S. (1994). Cloned glutamate receptors. Annu. Rev. Neurosci. *17*, 31–108.

Holm, M.M., Lunn, M.L., Traynelis, S.F., Kastrup, J.S., and Egebjerg, J. (2005). Structural determinants of agonist-specific kinetics at the ionotropic glutamate receptor 2. Proc. Natl. Acad. Sci. USA *102*, 12053–12058.

Huang, N., Banavali, N.K., and MacKerell, A.D., Jr. (2003). Protein-facilitated base flipping in DNA by cytosine-5-methyltransferase. Proc. Natl. Acad. Sci. USA *100*, 68–73.

Humphrey, W., Dalke, A., and Schulten, K. (1996). VMD: Visual Molecular Dynamics. J. Mol. Graph. *14*, 33–38.

Isaac, J.T.R., Ashby, M., and McBain, C.J. (2007). The role of the GluR2 subunit in AMPA receptor function and synaptic plasticity. Neuron *54*, 859–871.

Jorgensen, W.L., Chandrasekhar, J., Madura, J.D., Impey, R.W., and Klein, M.L. (1983). Comparison of simple potential functions for simulating liquid water. J. Chem. Physiol. *79*, 926–935.

Kristiansen, L.V., Huerta, I., Beneyto, M., and Meador-Woodruff, J.H. (2007). NMDA receptors and schizophrenia. Curr. Opin. Pharmacol. *7*, 48–55.

Kumar, S., Rosenberg, J.M., Bouzida, D., Swendsen, R.H., and Kollman, P.A. (1992). The weighted histogram analysis method for free-energy calculations on biomolecules. I. The method. J. Comput. Chem. *13*, 1011–1021.

Kuusinen, A., Arvola, M., and Keinänen, K. (1995). Molecular dissection of the agonist binding site of an AMPA receptor. EMBO J. *14*, 6327–6332.

MacKerell, A.D., Jr., Bashford, D., Bellott, M., Dunbrack, R.L., Jr., Evanseck, J.D., Field, M.J., Fischer, S., Gao, J., Guo, H., Ha, S., et al. (1998). All-atom empirical potential for molecular modeling and dynamics studies of proteins. J. Phys. Chem. B *102*, 3586–3616.

Madden, D.R. (2002). The structure and function of glutamate receptor ion channels. Nat. Rev. Neurosci. *3*, 91–101.

Madden, D.R., Armstrong, N., Svergun, D., Perez, J., and Vachette, P. (2005). Solution X-ray scattering evidence for agonist- and antagonist-induced modulation of cleft closure in a glutamate receptor ligand-binding domain. J. Biol. Chem. *280*, 23637–23642.

Mamonova, T., Hespenheide, B., Straub, R., Thorpe, M.F., and Kurnikova, M. (2005). Protein flexibility using constraints from molecular dynamics simulations. Phys. Biol. *2*, S137–S147.

Mayer, M.L. (2006). Glutamate receptors at atomic resolution. Nature *440*, 456–462.

Mayer, M.L., Ghosal, A., Dolman, N.P., and Jane, D.E. (2006). Crystal structures of the kainate receptor GluR5 ligand binding core dimer with novel GluR5-selective antagonists. J. Neurosci. *26*, 2852–2861.

McFeeters, R.L., and Oswald, R.E. (2002). Structural mobility of the extracellular ligand-binding core of an ionotropic glutamate receptor. Analysis of NMR relaxation dynamics. Biochemistry *41*, 10472–10481.

McFeeters, R.L., and Oswald, R.E. (2004). Emerging structural explanations of ionotropic glutamate receptor function. FASEB J. *18*, 428–438.

Mendieta, J., Gago, F., and Ramírez, G. (2005). Binding of 5′-GMP to the GluR2 AMPA receptor: insight from targeted molecular dynamics simulations. Biochemistry *44*, 14470–14476.

Nakagawa, T., Cheng, Y., Ramm, E., Sheng, M., and Walz, T. (2005). Structure and different conformational states of native AMPA receptor complexes. Nature *433*, 545–549.

O'Neill, M.J., and Witkin, J.M. (2007). AMPA receptor potentiators: application for depression and Parkinson's disease. Curr. Drug Targets *8*, 603–620.

O'Neill, M.J., Bleakman, D., Zimmerman, D.M., and Nisenbaum, E.S. (2004). AMPA receptor potentiators for the treatment of CNS disorders. Curr. Drug Targets CNS Neurol. Disord. *3*, 181–194.

Ramanoudjame, G., Du, M., Mankiewicz, K.A., and Jayaraman, V. (2006). Allosteric mechanism in AMPA receptors: a FRET-based investigation of conformational changes. Proc. Natl. Acad. Sci. USA *103*, 10473–10478.

Ravindranathan, K.P., Gallicchio, E., and Levy, R.M. (2005). Conformational equilibria and free energy profiles for the allosteric transition of the ribose-binding protein. J. Mol. Biol. *353*, 196–210.

Richards, F.M. (1977). Areas, volumes, packing and protein structure. Annu. Rev. Biophys. Bioeng. *6*, 151–176.

Robert, A., Armstrong, N., Gouaux, J.E., and Howe, J.R. (2005). AMPA receptor binding cleft mutations that alter affinity, efficacy, and recovery from desensitization. J. Neurosci. *25*, 3752–3762.

Rogers, S.W., Andrews, P.I., Gahring, L.C., Whisenand, T., Cauley, K., Crain, B., Hughes, T.E., Heinemann, S.F., and McNamara, J.O. (1994). Autoantibodies to glutamate receptor GluR3 in Rasmussen's encephalitis. Science *265*, 648–651.

Roux, B., and Schulten, K. (2004). Computational studies of membrane channels. Structure *12*, 1343–1351.

Ryckaert, J.-P., Ciccotti, G., and Berendsen, H.J.C. (1977). Numerical integration of cartesian equations of motion of a system with constraints: molecular dynamics of n-alkanes. J. Comput. Physiol. *23*, 327–341.

Schorge, S., and Colquhoun, D. (2003). Studies of NMDA receptor function and stoichiometry with truncated and tandem subunits. J. Neurosci. *23*, 1151–1158.

Smolin, N., and Winter, R. (2004). Molecular dynamics simulations of staphylococcal nuclease: properties of water at the protein surface. J. Phys. Chem. B *108*, 15928–15937.

Souaille, M., and Roux, B. (2001). Extension to the weighted histogram analysis method: combining umbrella sampling with free energy calculations. Comput. Phys. Comm. *135*, 40–57.

Speranskiy, K., and Kurnikova, M. (2005). On the binding determinants of the glutamate agonist with the glutamate receptor ligand binding domain. Biochemistry *44*, 11508–11517.

Stern-Bach, Y., Bettler, B., Hartley, M., Sheppard, P.O., O'Hara, P.J., and Heinemann, S.F. (1994). Agonist selectivity of glutamate receptors is specified by two domains structurally related to bacterial amino acid-binding proteins. Neuron *13*, 1345–1357.

Stryer, L., and Haugland, R.P. (1967). Energy transfer: a spectroscopic ruler. Proc. Natl. Acad. Sci. USA *58*, 719–726.

Svergun, D., Barberato, C., and Koch, M.H.J. (1995). CRYSOL - a program to evaluate X-ray solution scattering of biological macromolecules from atomic coordinates. J. Appl. Cryst. *28*, 768–773.

Svergun, D.I., Richard, S., Koch, M.H., Sayers, Z., Kuprin, S., and Zaccai, G. (1998). Protein hydration in solution: experimental observation by x-ray and neutron scattering. Proc. Natl. Acad. Sci. USA *95*, 2267–2272.

Tichelaar, W., Safferling, M., Keinänen, K., Stark, H., and Madden, D.R. (2004). The three-dimensional structure of an ionotropic glutamate receptor reveals a dimer-of-dimers assembly. J. Mol. Biol. *344*, 435–442.

Torrie, G.M., and Valleau, J.P. (1977). Nonphysical sampling distributions in Monte Carlo free-energy estimation: umbrella sampling. J. Comput. Physiol. *23*, 187–199.

Valentine, E.R., and Palmer, A.G., III. (2005). Microsecond-to-millisecond conformational dynamics demarcate the GluR2 glutamate receptor bound to agonists glutamate, quisqualate, and AMPA. Biochemistry *44*, 3410–3417.

Voss, N.R., Gerstein, M., Steitz, T.A., and Moore, P.B. (2006). The geometry of the ribosomal polypeptide exit tunnel. J. Mol. Biol. *360*, 893–906.

Woo, H.-J., and Roux, B. (2005). Calculation of absolute protein-ligand binding free energy from computer simulations. Proc. Natl. Acad. Sci. USA *102*, 6825–6830.

Wriggers, W., and Schulten, K. (1997). Protein domain movements: detection of rigid domains and visualization of hinges in comparisons of atomic coordinates. Proteins *29*, 1–14.

 

# Flexibility of a Glutamate-Binding Domain

Robert E. Oswald[1,*]
[1]Department of Molecular Medicine, Cornell University, Ithaca, NY 14853, USA
*Correspondence: reo1@cornell.edu
DOI 10.1016/j.str.2007.09.005

**The molecular dynamics simulation of the binding domain of a glutamate receptor presented in this issue of *Structure* (Lau & Roux, 2007) provides insights into large-scale fluctuations of this protein that are supported by experiment and provide constraints on possible models for the function of the intact glutamate receptor.**

Glutamate receptors are the major excitatory neurotransmitter receptors in the mammalian central nervous system and are involved in a range of neurological diseases (Parkinson's and Alzheimer's diseases, Huntington's chorea, and epilepsy) and in normal physiological processes, such as learning and memory. Drugs targeted to these receptors have enormous potential for treating neurological and psychiatric disorders. One of the important breakthroughs in the study of these receptors was the isolation of a soluble binding domain and the solution of the crystal structure (Armstrong et al., 1998). Although the binding domain represents an isolated portion of the intact protein, it binds agonists and antagonists with an affinity similar to the intact protein and has become an important model system for understanding the relationship between the structure and dynamics of the binding domain and the overall function of the protein. The crystal structures have provided a wealth of information on the structure of the binding site and have suggested clues to the coupling between binding, channel opening, and desensitization. However, the crystal structures are largely static and may, in some cases, be affected by crystal packing. Obviously, it is the motion of the protein that provides the initial signal that is transmitted to the ion channel and considerable effort has been made to understand the solution behavior of the binding domain using NMR spectroscopy (Ahmed et al., 2007), FTIR spectroscopy (Cheng et al., 2002), fluorescence spectroscopy (Abele et al., 2000), and small-angle X-ray scattering (Madden et al., 2005), as well as computational methods (Arinaminpathy et al., 2002; Mamonova et al., 2005). Each of these methods has provided new information highlighting different aspects of the structure and dynamics of this important protein. The protein consists of two lobes that are often assumed to move as rigid bodies, with the ligand-binding site between the two lobes. Upon binding of agonist, the lobes close and envelope the ligand, and a modest correlation has been observed between the degree of lobe closure in some crystal structures and the efficacy of an agonist. However, even the crystal structures suggest that the relative lobe orientation is not static. NMR (A.S. Maltsev and R.E.O., unpublished data), fluorescence (Ramanoudjame et al., 2006), and small-angle X-ray measurements (Madden et al., 2005) report on the average solution structure, which is in some cases, different from the crystal structure.

Lau and Roux (2007) used all-atom molecular dynamics in conjunction with umbrella sampling to compute the free energy landscape of the binding domain in the apo state, bound to an anagonist (DNQX) and bound to the natural ligand (glutamate). Two distances (ξ1 and ξ2; Figure 1) were defined between the lobes (defined by the center of mass of groups of 2–3 sequential residues in each lobe) that capture the degree of lobe closure and possible twists of one lobe relative to the other, and the starting coordinates for the umbrella sampling were positioned along ξ1 and ξ2. The overall results are completely consistent with previous experiments and simulations, but do add important details. That is, the free energy landscapes (described by the [ξ1,ξ2] order parameter) suggest a protein for which the relative orientation of the two lobes in the apo state is extremely flexible, somewhat less flexible in the antagonist-bound state, and relatively, but not completely, rigid in the full agonist-bound state. In fact, the results suggest that, in the apo state, the relative orientation of the two lobes can be considerably more open than that observed in the apo crystal structure (Figure 1). This hyperextension of the structure has been observed in the crystal structure of an antagonist-bound form (Kasper et al., 2006) but has not yet been observed directly in an apo crystal structure. However, as described in the paper, ensemble average scatter profiles calculated from the simulation trajectories match the small-angle X-ray scattering data (Madden et al., 2005) better than profiles computed from the crystal structures, suggesting that in solution these hyperextended forms may exist. These results are also consistent with $^{19}$F NMR data (Ahmed et al., 2007), which show clearly that the apo form is very flexible. This is inferred from the dynamics of the four $^{19}$F-labeled tryptophans, one of which is in the cleft between the two lobes. In the case of a similar antagonist (CNQX), the tryptophan in the cleft shows at least two different states, and for the glutamate-bound form, this tryptophan is relatively rigid.

Another interesting result of these studies is a suggestion as to the steps in the binding process, which potentially represent the reaction coordinate. Again, at least on a superficial level, the results are consistent with experiment. The idea that binding first occurs to lobe 1 (docking) followed by closure of lobes and interaction with

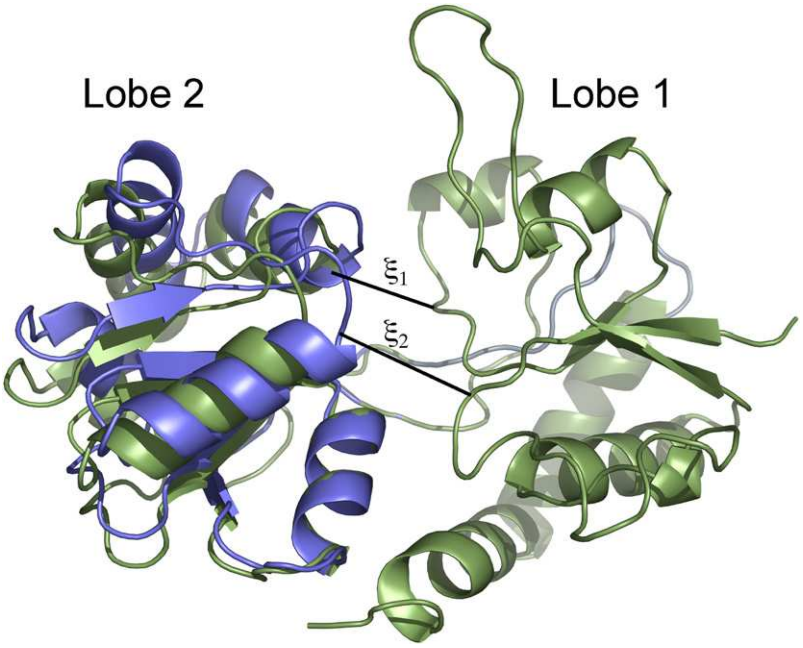


**Figure 1. Structures of the S1S2 GluR2 Protein with the Two Lobes Opened by 16° (Blue) and 30° (Green) Relative to the Glutamate-Bound Structure, 1FTJ**
This represents the range of openings represented by 91% of the conformational ensemble. The two distances shown ($\xi_1$ and $\xi_2$) were used to determine the two-dimensional order parameter.

lobe 2 (locking) has been proposed previously (Abele et al., 2000), but these simulations present a plausible pathway leading from the open state through two intermediates to a closed and fully bound state. Furthermore, the energetics of the process (stabilization of 9–12 kcal/mol) is similar to that obtained with isothermal titration calorimetry (approximately 8 kcal/mol, Madden et al., 2000).

The main interest in the motions of this protein is the idea that the closure of the lobes around the agonist forms the first step in the process leading to the opening of the ion channel. The receptor is formed from four subunits, each of which contains a copy of the S1S2 binding domain. Results from single channel recording at varying agonist concentrations have led to the notion that the conductance level of the channel may be correlated with the number of binding sites occupied, but it is not clear if simple closure of the lobes directly opens a conducting path in the ion channel or if lobe closure increases the probability that the channel will open, with other parts of the protein contributing essential roles (Oswald, 2004). Partial agonists, which in some cases bind with high affinity, preferentially populate lower conductance states. Extension of these studies to the free energy landscapes for partial agonists will be of considerable value for restraining possible models of channel activation.

## REFERENCES

Abele, R., Keinanen, K., and Madden, D.R. (2000). J. Biol. Chem. *275*, 21355–21363.

Ahmed, A.H., Loh, A.P., Jane, D.E., and Oswald, R.E. (2007). J. Biol. Chem. *282*, 12773–12784.

Arinaminpathy, Y., Sansom, M.S., and Biggin, P.C. (2002). Biophys. J. *82*, 676–683.

Armstrong, N., Sun, Y., Chen, G.Q., and Gouaux, E. (1998). Nature *395*, 913–917.

Cheng, Q., Thiran, S., Yernool, D., Gouaux, E., and Jayaraman, V. (2002). Biochemistry *41*, 1602–1608.

Kasper, C., Pickering, D.S., Mirza, O., Olsen, L., Kristensen, A.S., Greenwood, J.R., Liljefors, T., Schousboe, A., Watjen, F., Gajhede, M., et al. (2006). J. Mol. Biol. *357*, 1184–1201.

Lau, A.Y., and Roux, B. (2007). Structure *15*, this issue, 1203–1214.

Madden, D.R., Abele, R., Andersson, A., and Keinanen, K. (2000). Eur. J. Biochem. *267*, 4281–4289.

Madden, D.R., Armstrong, N., Svergun, D., Perez, J., and Vachette, P. (2005). J. Biol. Chem. *280*, 23637–23642.

Mamonova, T., Hespenheide, B., Straub, R., Thorpe, M.F., and Kurnikova, M. (2005). Phys Biol. *2*, S137–S147.

Oswald, R.E. (2004). Adv. Protein Chem. *68*, 313–349.

Ramanoudjame, G., Du, M., Mankiewicz, K.A., and Jayaraman, V. (2006). Proc. Natl. Acad. Sci. USA *103*, 10473–10478.

 